



## Robust Feedback Linearization Control of Air-Feed System in PEM Fuel Cell against Practical Uncertainty

Seyed Mehdi RAKHTALA<sup>1</sup>, Abolfazl RANJBAR<sup>2</sup>

<sup>1</sup>Assistant Prof. of Golestan University, Department of Electrical Engineering, Gorgan, Iran.

<sup>2</sup>Associated Prof. of Babol Noshirvani University of Technology, Babol, Iran.  
Sm.rakhtala@gu.ac.ir

**Abstract:** In this paper robust feedback linearization control approach based on the gap metric analysis is proposed to control a Proton Exchange Membrane Fuel Cell (PEMFC). The oxygen excess ratio is regulated through adjustment of the air supply to avoid oxygen starvation. Furthermore, the oxygen excess ratio regulation improves the efficiency whilst more net power will be delivered. In this paper a six order state variables PEM fuel cell is used as a plant whereas the system variations and disturbances are regarded as uncertainties to configure the perturbed plant. The gap metric analysis is gained in this paper to assess the difference between the perturbed plants and that of the nominal. Results of using the nonlinear control law reveal that the proposed feedback linearization control is robust against disturbances during the oxygen excess ratio regulation. Results verify that the measurement delays in super twisting algorithm excite un-modeled dynamics because of higher frequency in the oscillations. The proposed controller eliminates influence of un-modeled dynamic and delay of actuator and sensor. Furthermore the designed controller is found capable to attenuate the practical measurement noise effect (in terms of a stochastic uncertainty) in both of the frequency spectrum and also in the overall amplitude.

**Keywords:** PEM Fuel Cell, oxygen excess ratio, stochastic uncertainty, robust feedback linearization, gap metric.

### 1. Introduction

Fuel cell is an electrochemical device which generates electricity through reaction between hydrogen and oxygen [1]. Due to outstanding characteristics such as high energy efficiency, profitable to the environment, high power density, fast power response, low noise pollution and flexible modular structure, fuel cells attracted several interests of researchers [1]. PEMFC is a nonlinear dynamical system under different chemical, mechanical and electrical regimes. The model needs to express liquid/vapor/gas mixed flow transportation, heat conduction and electrochemical reaction. In order to the chemical reaction takes place a certain amount of the air supply is needed. In the literature this is called the oxygen excess ratio, i.e. ratio of the input oxygen flow over the reacted oxygen flow in the cathode. The reacted oxygen is highly dependent to the load variation. This means the inlet air flow is variable with the load changes. This is called the breathing of the fuel cell which is a vital key to avoid the hot spot occurrence. Meanwhile evaluation of the reacted oxygen needs some formula manipulation which is called the oxygen stoichiometry. The variation in the load current also changes speed of electrochemical reaction. When the oxygen flow rate in the cathode is too low, the power

output of fuel cell and also the voltage are reduced such that a so-called oxygen starvation happens. The oxygen starvation in the worse situation will lead to creating a hot spot on the membrane and will degrade the fuel cell. Thus, to prevent the membrane damage and oxygen depletion and the voltage drop, an effective control procedure is required to achieve an optimal inlet air flow rate. In fact to overcome the oxygen starvation,  $\lambda_{O_2}$  must be tuned in a desired constant amount through providing the air by a compressor [2]. The air-feed system of a PEMFC includes a motorized air compressor through a supply manifold to the cathode [3]. Its performance affects the dynamic and transient response when a sudden change in the load occurs. Fuel cell fails to tolerate oscillations and pulse changes in the pressure and air flow. Therefore a quality controller of the compressor is required to accurately control the air-feed system. This means that control of the compressor plays a main role in the performance of PEMFC. In recent years, several control strategies are proposed to control the fuel cell system. Pukrushpan et al. [4] implemented an observer-based feedback controller to protect the fuel cell stack from the oxygen starvation during changes in the current load. Further Pukrushpan et al. [5, 6], proposed a linearization based method via feedback and feed-forward controllers to adjust the flow rate of compressor in the PEMFC air supply system.

Grujicic and colleagues et al.[7] presented a model-based control strategy to optimize the transient behavior of a PEM fuel cell system including air and fuel supply subsystems. Shortcoming of classic methods and the linear design strategy lead to find accurate knowledge about parameters of the system or estimation of uncertainties. Severe nonlinearity of the system, modeling error and parametric uncertainties such as exhaustion of fuel cell components and fluctuations of environmental condition are some challenges in the adjustment approach. W. Na and colleagues et al. [8, 9] proposed a nonlinear controller for the nonlinear model of PEM fuel cell. The proposed controller is found effective to adjust the pressure in both sides of Membrane Electrode Assembly (MEA) to prolong the stack life. Rodatz et al. [10] proposed a dynamic model of air supply to design a Linear Quadratic Gaussian (LQG) controller. Simulation results of pressure trace confirms fast response time and also better transient responses together with disturbance rejection in comparison with the conventional PI controller. Due to fast variation of the dynamic, a nonlinear controller is found more beneficial. Niknezhadi and Kunusch et al. 2010 [11] also proposed LQR/LQG technique to regulate  $\lambda_{O_2}$ . The proposed LQG design necessitates linearizing a model about given (stationary) operating point using its first derivative (Jacobian matrix) of the Taylor series. However the performance of the design is found satisfactory in absence of neither sudden load disturbances nor uncertainty. The research by Garcia-Gabin et al. [12] confirms the statement during control of oxygen stoichiometry (via  $\lambda_{O_2}$ ). Nonetheless sliding mode controller produces chattering phenomenon that is destructive for mechanical systems. Since oscillatory angular velocity leads to oscillation in the outlet air flow of the compressor, this again leads to oscillation in the stoichiometry and also total performance of the fuel cell. Talj et al. [13-15] successfully used nonlinear sliding mode controllers of the compressor gaining a reduced four-order model through a cascade control structure in the inner loop and also during the breathing in the outer loop. In parallel simplified and reduced model in [13-15] provides a good structure to design nonlinear controller. However this is not formally validated in all range of the operating region. Meanwhile Kunusch et al. [16-18] in 2009 and 2010, proposed a second order sliding mode controller in the air supply to prevent the starvation. In this case, a super twisting algorithm stabilizes and prevents the chattering phenomena. This idea guarantees performance of the controller in a wider interval of the operation. A shortcoming of Talj et al. [13-15] and Kunusch et al. [16-18] works is the necessity for the oxygen flow meter in the cathode side to control  $\lambda_{O_2}$ . The transducer produces a delay of 1-2 seconds. The requirement is therefore modified by Kunusch et al. 2009 [16], 2010 [18] and 2013 [19] and in parallel by Talj research team et al. [14] in 2009 and 2010 [15, 19] to regulate  $\lambda_{O_2}$  assuming constant humidity. The oxygen ratio is then evaluated using the stoichiometry

formulation. A major lack of the research is using a direct measurement of the inlet oxygen. This is because the transducer augments another dynamic over the fuel cell system. Meanwhile, using lower accurate and expensive transducer are some other drawbacks which must be dealt. As another challenge, environment conditions variations and also the aging of the fuel cell cause uncertainty. These together with highly nonlinearity in the model require a quality controller design to take into account parametric uncertainty which necessitate designing a robust controller. Accordingly, Kunush et al. [16, 20] deal with parametric uncertainties, although dynamic of supply manifold pressure is ignored. Consequently, a static relation between optimal oxygen excess ratio and the compressor flow rate reference is established whilst the validity is questioned. An optimal ratio ( $\lambda_{O_2}$ ) is assessed between 2 and 2.4 to provide maximum net power  $P_{net}$  of the Fuel cell considering the tolerable stack current ( $I_{st}$ ) [21]. During the design procedure a 6-order model [22, 23] of PEM fuel cell together with a nonlinear dynamic of the air-feed system is considered here. The inlet air flow is regarded as a measured output whilst the load current and the motor voltage are regarded as disturbance and control input respectively. A robust feedback linearization control approach based on the gap metric analysis is proposed to stabilize  $\lambda_{O_2}$  at a desired optimal point. The gap metric approach is well gained to evaluate the discrepancy of the model from the proposed nominal plant.

This paper is organized as follows: in section 2, fuel cell is briefly described whilst analytic single-input single-output (SISO) model is presented. In section 3, an output feedback linearization is designed based on the nonlinear dynamic PEMFC model and the gap metric method. Robust feedback linearization control theorems are briefly introduced and applied to design  $H_\infty$  controllers. Simulation results are given in section 4 to show the performance of the proposed scheme against un-modeled dynamic as well as stochastic one. The latter uses a practical measurement noise on the ambient temperature. Finally, the work ends with a conclusion in section 5.

## 2. State Space Equations of PEMFC

Auxiliary equipment in combination with PEM fuel cell stack develops a nonlinear model. This includes following subsystems:

- Compressor dynamic model
- Air supply manifold model
- Cathode model
- Fuel cell stack model

State variables are defined as  $x = [\omega_{cp} \ P_{sm} \ m_{sm} \ m_{O_2} \ m_{N_2} \ P_{rm}]^T$

whilst model variables are defined in **Hata! Başyuru kaynağı bulunamadı..** Details of the model and relevant assumptions are completely studied in [22, 23].

Accordingly, the following nonlinear model of the fuel cell is considered where parameters are given in tables 2-4 in the appendix I.

**Table 1:** Key variables description

States	Unit	Definition
$x_1 = \omega_{cp}$	[rad / sec]	Angular speed of the compressor motor
$x_2 = P_{sm}$	[Pa]	Pressure in the supply manifold
$x_3 = m_{sm}$	[kg]	Air mass in the supply manifold
$x_4 = m_{O_2}$	[kg]	Oxygen mass in the cathode
$x_5 = m_{N_2}$	[kg]	Nitrogen mass in the cathode
$x_6 = P_{rm}$	[Pa]	Return manifold pressure
$u = v_{cm}$	[V]	Voltage of the DC motor (control input)
$d = I_{st}$	[A]	Total stack current
$M_a^{am} = y_{O_2,in} M_{O_2} + (1-y_{O_2,in}) M_{N_2}$		Molar mass
$P_{v,ca} = \frac{m_{v,ca,max} R_v T_{fc}}{V_{ca}}$		Vapor pressure in the cathode

$$\dot{x}_1 = \frac{\eta_{cm}}{J_{cp}} \frac{k_t}{R_{cm}} (v_{cm} - k_v x_1) - \frac{\tau_{cp}}{J_{cp}} \tag{1}$$

$$\begin{aligned} \dot{x}_2 = & \frac{\gamma R_a}{V_{sm}} (-K_{sm,out} x_2 + K_{sm,out} P_{v,ca} + K_{sm,out} \frac{x_5}{M_{N_2}} c_1 + K_{sm,out} \frac{x_4}{M_{O_2}} c_2) \frac{\gamma x_2}{x_3} \\ & + W_{cp} (T_{atm} + \frac{T_{am}}{\eta_{cp}} (\frac{x_2}{P_{atm}})^{\frac{\gamma-1}{\gamma}} - 1) \end{aligned} \tag{2}$$

$$\dot{x}_3 = W_{cp} - K_{sm,out} x_2 + K_{sm,out} P_{v,ca} + K_{sm,out} \frac{x_5}{M_{N_2}} c_1 + K_{sm,out} \frac{x_4}{M_{O_2}} c_2 \tag{3}$$

$$\begin{aligned} \dot{x}_4 = & -\frac{x_4}{x_4 + x_5 + c_3} K_{ca,out} (-x_6 + P_{v,ca} + \frac{x_5}{M_{N_2}} c_1 + \frac{x_4}{M_{O_2}} c_2) + y_{O_2,in} K_{sm,out} \\ & (x_2 - \frac{x_4}{M_{O_2}} c_2 - P_{v,ca} - \frac{x_5}{M_{N_2}} c_1) - n \frac{M_{O_2}}{4F} I_{st} \end{aligned} \tag{4}$$

$$\begin{aligned} \dot{x}_5 = & (1 - X_{O_2,in}) (1 + \Omega_{am})^{-1} K_{sm,out} (x_2 - \frac{x_4}{M_{O_2}} c_2 - \frac{x_5}{M_{N_2}} c_1 - P_{v,ca}) - \frac{x_5}{x_4 + x_5 + c_3} K_{ca,out} \\ & (-x_6 + \frac{x_4}{M_{O_2}} c_2 + \frac{x_5}{M_{N_2}} c_1 + P_{v,ca}) \end{aligned} \tag{5}$$

$$\begin{aligned} \dot{x}_6 = & \frac{R_a T_{rm}}{V_{rm}} (K_{ca,out} (\frac{x_4}{M_{O_2}} c_2 + \frac{x_5}{M_{N_2}} c_1 + P_{v,ca} - x_6) - \\ & (P_{a_6} x_6^5 + P_{a_5} x_6^4 + P_{a_4} x_6^3 + P_{a_3} x_6^2 + P_{a_2} x_6 + P_{a_1})) \end{aligned} \tag{6}$$

Where  $\tau_{cm}$  is the motor torque,  $k_t$ ,  $R_{cm}$  and  $k_v$  are motor constants and  $\eta_{cm}$  is the motor mechanical efficiency. Meanwhile  $\tau_{cp}$  is the load torque which is expressed as in the following [24]:

$$\begin{aligned} \tau_{cp} = & \frac{\pi}{30} (\alpha_0 + \alpha_1 x_1 + \alpha_{00} + \alpha_{10} x_1 + \alpha_{20} (x_1)^2 \\ & + \alpha_{01} x_2 + \alpha_{11} x_2 x_1 + \alpha_{02} (x_2)^2) \end{aligned} \tag{7}$$

Where  $W_{cp}$  is the delivered air mass flow by compressor. This variable may be represented in the following form [24]:

$$W_{cp} = \beta_{00} + \beta_{10} x_2 + \beta_{20} (x_2)^2 + \beta_{01} x_1 + \beta_{11} x_2 x_1 + \beta_{02} (x_1)^2 \tag{8}$$

Furthermore, the humidity ratio  $\Omega_{am}$  is given by

$$\Omega_{am} = \frac{M_v}{M_a^{am}} \frac{\Phi_{am} P_{sat,T_{am}}}{P_{atm}} \left( 1 - \frac{\Phi_{am} P_{sat,T_{am}}}{P_{atm}} \right)^{-1}$$

A reference values for PEMFC model parameters are given in **Hata! Başvuru kaynağı bulunamadı., Hata! Başvuru kaynağı bulunamadı., and Hata! Başvuru kaynağı bulunamadı.** of Appendix I [22, 23]. Equations (1) - (6) can be rewritten in the following general form where  $x \in \mathbb{R}^6$  is state of the system;  $f \in \mathbb{R}^6 \rightarrow \mathbb{R}^6$  is appropriate continuous vector function.

$$\dot{x} = \begin{bmatrix} f_1(x_1, x_2) \\ f_2(x_1, x_2, x_3, x_4, x_5) \\ f_3(x_1, x_2, x_4, x_5) \\ f_4(x_2, x_4, x_5, x_6) \\ f_5(x_2, x_4, x_5, x_6) \\ f_6(x_4, x_5, x_6) \end{bmatrix} + \begin{bmatrix} \eta_{cm} \frac{k_t}{J_{cp} R_{cm}} \\ 0 \\ 0 \\ 0 \\ 0 \\ 0 \end{bmatrix} v_{cm} + \begin{bmatrix} 0 \\ 0 \\ 0 \\ -n \frac{M_{O2}}{4F} \\ 0 \\ 0 \end{bmatrix} I_{st} \quad (9)$$

$f(x) \quad \begin{matrix} 4 & 4 & 2 & 4 & 4 & 3 \\ 4 & 2 & 4 & 4 & 3 \\ P(x) \end{matrix}$

### 3. The Oxygen Excess Ratio Control using Robust Feedback Linearization Technique

In this section primarily brief basics of the feedback linearization technique in nonlinear control design will be given (equation 10 - 14). The work will be developed when a load current changes (equation 15 - 20). The variation is regarded as a (measured) disturbance. Finally, a robust feedback linearization procedure will be introduced to cope with an uncertainty as the main aim of the manuscript (equation 21 - 27). The rest of the section will be devoted to a  $H_\infty$  design gaining the gap metric analysis. This technique is given to provide more comparative studies of those proposed robust techniques.

#### - Basics of the Feedback Linearization Technique

In the fuel cell system  $x = [\omega_{cp} \ P_{sm} \ m_{sm} \ m_{O2} \ m_{N2} \ P_{rm}]^T$  and  $u = v_{cm}$  indicates the state vector and the control signal respectively. The delivered air mass flow  $W_{cp}$  is regarded as an output function  $y = h(x) = W_{cp}$  whilst  $g(x)$

matrix is  $[\eta_{cm} \ \frac{k_t}{J_{cp} R_{cm}} \ 0 \ 0 \ 0 \ 0]^T$ . Gaining  $r$ -times differentiation of the output yields a linear input-output relation in the following form:

$$y^{(r)} = w \quad (10)$$

Where  $w$  is treated as a control. Output feedback linearization spots the relative degree of  $r$  if the control signal  $u_c$  appears after  $r$ -times differentiation of the output  $y$  as:

$$y^{(r)} = L_f^r h(x) + L_g L_f^{r-1} h(x) u_c \quad (11)$$

For  $L_g L_f^{r-1} h(x) \neq 0$ . Accordingly, this achieves the control signal of (10) by:

$$u_c(x, w) = \frac{1}{L_g L_f^{r-1} h(x)} (-L_f^r h(x) + w) \quad (12)$$

In the same procedure the relative degree of the output in (8) will be found using the following differentiation:

$$\frac{\partial h(x)}{\partial x} = \frac{\partial W_{cp}}{\partial x} = \frac{\partial (\beta_{00} + \beta_{10} x_2 + \beta_{20} (x_2)^2 + \beta_{01} x_1 + \beta_{11} x_2 x_1 + \beta_{02} (x_1)^2)}{\partial x} \quad (13)$$

$$\frac{\partial h(x)}{\partial x} L_f h(x) + L_g L_f^0 h(x) u_c = L_f h(x) + L_g L_f^0 h(x) v_{cm} \quad (14)$$

#### - In the Presence of a Measured Disturbance

The same procedure as in (15) assesses the relative degree of one when a measured disturbance  $d$  (i.e. the load current) is regarded as another input.

$$L_P L_f^i h(x) = 0 \text{ for } i < r-1 ; L_P L_f^{r-1} h(x) \neq 0 \rightarrow r \quad (15)$$

Using (12) immediately finds a counteracting control effort against the disturbance  $d$  as in the following for  $r=1$ :

$$u_c(x, w) = \frac{1}{L_g L_f^{r-1} h} (-L_f^r h + w - L_P L_f^{r-1} P(x) d) \quad (16)$$

Matrix  $P(x)$  is the input disturbance coefficient as denoted in the last term in (9), i.e.:  $P(x) = \begin{bmatrix} 0 & 0 & 0 & -n \frac{M_{O2}}{4F} & 0 & 0 \end{bmatrix}^T$ . The

control signal of the nonlinear system in presence of the measured disturbance is as follows:

$$u_c(x, w) = \frac{1}{L_g L_f^0 h} (-L_f h + w - L_P L_f^0 P(x) d) = \alpha_c(x) + \beta_c(x) w \quad (17)$$

The lie derivative of  $P(x)$  gives  $L_P L_f^0 P(x)$  equal zero. Therefore, the control signal  $u_c(x, w)$  is achieved by:

$$u_c(x, w) = \alpha_c(x) + \beta_c(x) w = \frac{1}{L_g L_f^0 h(x)} (-L_f h(x) + w) \quad (18)$$

Consequently,  $\alpha_c(x)$  and  $\beta_c(x)$  in (18) will be found as  $\alpha_c(x) = -(L_g h(x))^{-1} L_f h(x)$  and  $\beta_c(x) = (L_g L_f^0 h(x))^{-1} = (L_g h(x))^{-1}$ . Replacing parameters in Table 4 gives  $\alpha_c(x)$  and  $\beta_c(x)$  as in (19).

$$\begin{aligned} \alpha_c(x) &= (1.0 \times (1.0 \times (3.9 x_1 + (7.72 e 9 \times ((9.87 e - 6 \times x_2)^{(2/7)} - 1.0) \times (4.11 e - 10 \times x_1^2 + 3.55 e - 13 \times x_1 x_2 + 8.8 e - 16 \times x_2^2 + 4.83 e - 5)) / x_1) \times (8.22 e - 10 \times x_1 + 3.55 e - 13 \times x_2) \\ &\quad - (1.0 e - 5 \times (1.29 \times (9.87 e - 6 \times x_2)^{(2/7)} - 0.29) \times (0.00246 x_1^2 + 2.13 e - 6 \times x_1 x_2 + 5.26 e - 9 \times x_2^2 + 289.0) \\ &\quad + (1.0 e - 5 \times x_2 \times (46.6 x_4 - 5.08 e - 6 \times x_2 + 53.2 x_5 + 0.232)) \times x_3) \\ &\quad \times (3.55 e - 13 \times x_1 + 1.76 e - 15 \times x_2)) / (2.1 e - 7 \times x_1 + 9.06 e - 11 \times x_2) \\ \beta_c(x) &= 1 / (2.1 \times 10^{-7} \times x_1 + 9.06 \times 10^{-11} \times x_2) \end{aligned} \quad (19)$$

In comparison with the standard linearized system:

$$\dot{x}_c = A_c x_c + B_c w \quad (20)$$

Where  $A_c$  and  $B_c$  are the matrices of the Brunovsky canonical form,  $x_c$  is defined by  $x_c^T = [h(x) \ L_f h(x) \ L_f^2 h(x) \ \dots]$ .

#### - In the presence of uncertainty

The above technique of feedback linearization is found sensitive to model uncertainty [25]. To cope with, a robust feedback linearization is proposed to be used in the system operating point  $x_0$ . To distinguish two distinct cases, similar but different notations are used hereafter. A robust feedback linearization is shown by the following linear form:

$$\dot{x}_r = A_r x_r + B_r v \quad (21)$$

Similarly, a robust feedback linearization control law may be designed [26] by a control law of:  $u(x, w) = \alpha(x) + \beta(x) v$ , where  $v$  is the control law,  $A_r = \frac{\partial f(x_0)}{\partial x}$  and  $B_r = g(x_0)$  are correspondent to

appropriate linear approximation of the nonlinear terms. The operating point is chosen as [22]:

$$x_{1(0)}=5100; x_{2(0)}=1.48038; x_{3(0)}=0.03; x_{4(0)}=1.2 \times 10^{-3}; x_{5(0)}=0.008; x_{6(0)}=1.28300$$

. Matrices  $A_r$  and  $B_r$  are then achieved as:

$$A_r = \begin{bmatrix} -4.37 & -.562 \times 10^{-1} & 0 & 0 & 0 & 0 \\ 50.8 & -26.2 & .534 \times 10^7 & .235 \times 10^9 & .268 \times 10^9 & 0 \\ .714 \times 10^{-5} & -.363 \times 10^{-5} & 0 & 33.3 & 38.0 & 0 \\ 0 & .837 \times 10^{-6} & 0 & -13.3 & -11.8 & .337 \times 10^{-6} \\ 0 & .276e-5 & 0 & -36.1 & -44.5 & .139 \times 10^{-5} \\ 0 & 0 & 0 & .403 \times 10^9 & .460 \times 10^9 & -49 \end{bmatrix} \text{ and } B_r = \begin{bmatrix} 255 \\ 0 \\ 0 \\ 0 \\ 0 \\ 0 \end{bmatrix}$$

The notation for the feedback linearization is described here. Defining  $\phi_c^T = [h(x) \ L_f h(x) \ L_f^2 h(x) \ \dots \ L_f^{r-1} h(x)]$  and  $x_r = \phi(x)$ , yields  $\alpha(x)$  and  $\beta(x)$  in (18) of the robust control law as follows:

$$\alpha(x) = \alpha_c(x) + \beta_c(x) L T^{-1} \phi_c \tag{22}$$

$$\phi(x) = T^{-1} \phi_c(x)$$

$$\beta(x) = \beta_c(x) R^{-1}$$

$$\alpha(x) = \alpha_c(x) + \beta_c(x) L T^{-1} \phi_c \tag{23}$$

$$\beta(x) = \frac{2.24}{(0.906 \times 10^{-10} \times x_2 + 0.448 \times 10^{-2} \times x_1)}$$

Finally, the control law will be generated by:

$$u(x,w) = \alpha_c(x) + \beta_c(x) L T^{-1} \phi_c + \beta_c(x) R^{-1} v = \alpha(x) + \beta(x) v \tag{24}$$

Matrices  $L$ ,  $R$  and  $T$  matrices which are needed for the robust feedback linearization method are as follows:

$$L = -A(x_0) \frac{\partial(\alpha_c(x_0))}{\partial x}$$

$$T = \frac{\partial \phi_c(x_0)}{\partial x} \tag{25}$$

$$R = A^{-1}(x_0)$$

Where for the PEMC evaluated as:

$$L = 10^3 \times [ 0.5716 \ -2.3691 \ -1.25 \times 10^{-14} \ -2.45 \times 10^{-11} \ -2.80 \times 10^{-11} \ 0 ]$$

$$T = [ 0.0088 \ -1.05 \times 10^{-3} \ 0 \ 0 \ 0 \ 0 ] \tag{26}$$

$$R = 0.4461$$

As already stated the load current is regarded as a measurable disturbance  $d$  due to change in the operating point. Large and sudden load variation necessitates supplying huge amount of the air. Otherwise the lack of the air supply damages the membrane. In order to counteract an undesired change in the load, the control law in (24) is modified to (27) considering the term  $-\gamma(x) d$  in the control as:

$$u(x, w) = \alpha(x) + \beta(x) v - \gamma(x) d \tag{27}$$

$$\gamma(x) = A^{-1}(x) P(x)$$

$$u = \alpha_c(x) + \beta_c(x) L T^{-1} \phi_c + \beta_c(x) R^{-1} v - A^{-1}(x) P(x) d$$

### 3.1. Deviation from the nominal plant

Suppose that  $G_0$  denotes the nominal model of the fuel cell in the operating condition such that  $G_0 = \frac{N}{M}$  is a normalized coprime factorization of the weighted plant and  $M^* M^{*+} + N^* N^{*+} = I$ . Consider the deviation  $G_\Delta$  of the nominal plant which is defined as  $G_\Delta = \frac{N+\Delta_1}{M+\Delta_2}$  assuming [27, 28]:

$$\| \begin{bmatrix} \Delta_M & \Delta_N \end{bmatrix} \|_\infty < \epsilon \tag{28}$$

It should be noted that  $M$  and  $N$  are denominator and numerator polynomials of  $G_0$  respectively. A gap metric between the nominal plant  $G_0$  and the perturbed plant  $G_\Delta$  will be defined in the following section.

### 3.2. Choosing the nominal plant and assessing the gap metric Wang et al. [27, 28]

Minimum value of  $\| \begin{bmatrix} \Delta_M & \Delta_N \end{bmatrix} \|_\infty < \epsilon$  - that converts the nominal plant model of fuel cell  $G_0$  to the perturbed model  $G_\Delta$ ; is treated as a least distance of the current situation from the nominal plant so called the gap metric between  $G_0$  and  $G_\Delta$  i.e.  $\delta(G_0, G_\Delta)$ . Furthermore, the nominal plant is chosen such that the difference between the nominal and that of perturbed plant i.e. the maximum distance can be minimized as follows:

$$\min_{G_0} \max_{G_i} \delta(G_0, G_i) \tag{29}$$

Transfer functions of fuel cell in different operating points are derived according to different load currents of  $\frac{1}{0.001836}$  step and presented in **Hata! Başvuru kaynağı bulunamadı..** A gap metric evaluation of all transfer functions are presented in **Hata! Başvuru kaynağı bulunamadı..** From **Hata! Başvuru kaynağı bulunamadı..**, it can be seen that  $G_4$  is at the middle of those other transfer functions with similar distance (i.e. gap metric). Therefore, this is treated as a nominal plant of the fuel cell system during the robust control design. The widest gap metric between the nominal plant  $G_4$  and the rest, according to the criteria  $\min_{G_0} \max_{G_i} \delta(G_0, G_i)$  is also treated as the uncertainty bound (i.e. 0.0019).

### 3.3. Robust stability analysis

The designed robust control algorithm needs to guarantee the stability of the fuel cell system with respect to model uncertainties and disturbances. Consider the gain controller  $K$  as in Figure 1.

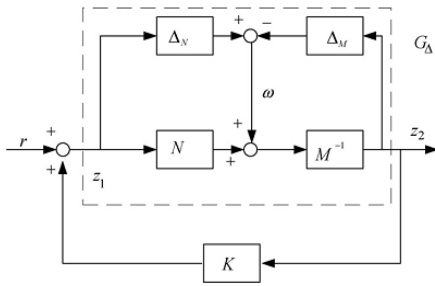


**Figure 1:** Closed-loop feedback structure of uncertain system using a controller  $K$  Wang et al. [27, 28]

Transfer function of systems is rearranged as follows:

$$\begin{bmatrix} z_1 \\ z_2 \end{bmatrix} = \begin{bmatrix} K \\ I \end{bmatrix} (I - GK)^{-1} M^{-1} \omega = \begin{bmatrix} K \\ I \end{bmatrix} (I - GK)^{-1} [I \ G] \omega \quad (30)$$

Where  $z_i, i=1,2$  and  $\omega$  are input and output signals of the system respectively. Using the small gain theorem [27-29], provides internal stability of the closed-loop system for all uncertainties with less magnitude than  $\|[\Delta_M \ \Delta_N]\|_\infty < \varepsilon$  if and only if:

$$\left\| \begin{bmatrix} K \\ I \end{bmatrix} (I - G_0 K)^{-1} M^{-1} \right\|_\infty = \left\| \begin{bmatrix} K \\ I \end{bmatrix} (I - G_0 K)^{-1} [I \ G_0] \right\|_\infty \leq \frac{1}{\varepsilon} \quad (31)$$

For the relative degree  $r=0$  the system is simplified as in Figure 2.

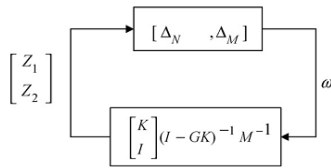


**Figure 2:** Closed-loop feedback configuration of system with  $r=0$  Wang et al. [27, 28]

**3.4. The stability margin**

The stability margin of  $b(G_0, K)$  for the closed loop system is found [27, 28] as follows:

$$b(G_0, K) = \left\| \begin{bmatrix} K \\ I \end{bmatrix} (I - G_0 K)^{-1} [I \ G_0] \right\|_\infty^{-1} \quad (32)$$

The closed-loop system is internally stable for all uncertainties  $\|[\Delta_M \ \Delta_N]\|_\infty < \varepsilon$  if and only if  $b(G_0, K) \geq \varepsilon$ .

Therefore, the goal of designing controller  $K$  for the nominal plant of fuel cell  $G_0$  is  $b(G_0, K) \geq 0.0019$ .

**3.5. Design of  $H_\infty$  loop-shaping robust controller**

In order to provide a robust stability and performance against the modeling error McFarlane-Glover method et al. [30] is used. Loop shaping method is chosen to achieve robust performance and stability in two different steps of the controller design procedure [30]. To design a loop-shaping based technique the following three steps must be taken:

**Step 1:**

Nominal plant of the fuel cell  $G_0$  with pre-weighting  $w_1$  and post-weighting  $w_2$  is converted to form of  $G_s = w_2 G_0 w_1$  (Figure 3).

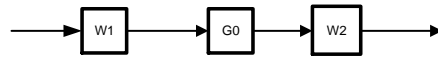


**Figure 3:** First step of the robust controller design Wang et al. [27, 28]

**Step 2:**

The maximum stability margin  $b_{max}$  can be calculated with the following relation:

$$b_{max}(G_s, K) = \left( \inf_K \left\| \begin{bmatrix} K \\ I \end{bmatrix} (I - G_s K)^{-1} [I \ G_s] \right\|_\infty \right)^{-1} \quad (33)$$

If  $b_{max}(G_s, K) = 1$  the algorithm returns back to step1 to redefine weightings  $w_1$  and  $w_2$ . Finally, if  $b_{max}(G_s, K) \geq \varepsilon$  is the stabilizing controller  $K_\infty$  must satisfy the following relation (Figure 4).

$$\left\| \begin{bmatrix} K_\infty \\ I \end{bmatrix} (I - G_s K_\infty)^{-1} [I \ G_s] \right\|_\infty^{-1} \geq \varepsilon \quad (34)$$

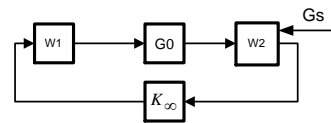


**Figure 4:** Second step of the robust controller design Wang et al. [27, 28]

**Step 3:**

The  $K_\infty$  controller is pre and post-multiplied by the weights. Thus  $K = w_1 K_\infty w_2$  controls the fuel cell with nominal model  $G_0$  according to Figure 5. The  $H_\infty$  controller is designed according to physical characteristics of system and desired performance. In the first step pre and post-weights must be determined. It is required that the gain  $G_s = W_2 G_0 W_1$  must be high enough at frequency where the disturbance attenuation is needed. Similarly, the gain is required to be low enough at frequency where the robust stability is of interest. By a trial and error, weights of the sensitivity functions are achieved  $w_1 = \frac{s+1}{s}$  and  $w_2 = I$ . Accordingly, the controller  $K_\infty$  is yielded as in equation (35):

$$K_\infty = \frac{(1.207(s+4096)(s+88.94)(s+88.93)(s+39.53)(s+39.49)(s+3.92) \times (s+3.029)(s+3.026)(s+1)(s^2+2.004s+1.016)(s^2+1.533s+0.6529))}{((s+4096)(s+88.94)(s+88.93)(s+39.53)(s+39.49)(s+3.92)(s+3.029) \times (s+3.026)(s+1.707)(s+0.7071)(s^2+2.004s+1.016)(s^2+1.533s+0.6529))} \quad (35)$$

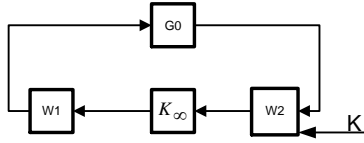


Figure 5: Third step of the robust controller design Wang et al. [27, 28]

In the second step,  $K_\infty$  controller is multiplied by weighting functions as  $K=W_1(s) K_\infty(s) W_2(s)$ . The designed controller  $\kappa$  is applied on the fuel system according to the structure in Figure 6. The aim is to adjust the air mass flow  $w_{cp}$  in (8) which is treated as a desired output, i.e.:

$$y=h(x)=W_{cp}=\beta_{00}+\beta_{10}x_2+\beta_{20}(x_2)^2+\beta_{01}x_1+\beta_{11}x_2x_1+\beta_{02}(x_1)^2 \quad (36)$$

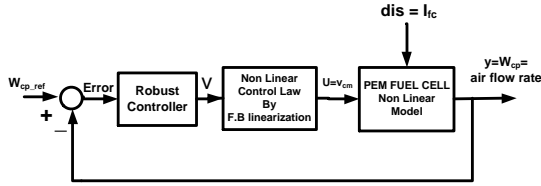


Figure 6: Structure of the fuel cell system using robust feedback linearization control

Assuming fixed humidification  $w_{air,in}$  is directly relevant to  $w_{cp}$  through the supply manifold dynamic. In the current work, the error is defined as follows:

$$e=w_{cp}-w_{air,ref} \quad (37)$$

Where  $w_{air,ref}$  is the air mass flow reference according to:

$$w_{air,ref}=\frac{M_{O_2} n I_{st}}{4 F} \lambda_{opt} (1+\Omega_{atm}) \frac{1}{M_a^{atm}} \quad (38)$$

Denoting  $\Omega_{atm}$  as the relative humidity of the air. However, the relation between the optimal oxygen ( $\lambda_{opt}$ ) and the reference value for the air mass is obtained as follows [16]:

$$\lambda_{opt}=\frac{w_{air,ref}}{\frac{M_{O_2} n I_{st}}{4 F} (1+\Omega_{atm}) \frac{1}{M_a^{atm}}} \quad (39)$$

Indeed, tuning  $\lambda_{o_2}$  in the optimal value  $\lambda_{opt}$  ensures the required performance.

### 4. Simulation results

In order to verify the performance and efficiency of the closed-loop system, two methods of robust feedback linearization and second order sliding mode controller with super twisting algorithm are gained in different

conditions. Primarily a simulation is made in section one when no measurement delay in  $W_{cp}$  is of concerned. Second section deals with the measurement delay in  $W_{cp}$ . Effects of un-modeled dynamic and the delay are investigated to evaluate performance of the super twisting algorithm. Finally, the last part assesses capability of the robust feedback linearization against the model uncertainty.

The nonlinear model is expressed in equations (1) to (6) for a 75 kW fuel cell stack supplied with a 14 kW motor compressor to provide the required air. All simulations are performed with ODE4 Runge-Kutta solver using fixed step size of 1ms. Performance of the proposed robust feedback linearization controller in the closed loop will be assessed against the load variation and parametric uncertainty in the following.

#### 4.1.Effect of the controller against wide range of the load variation

The effect of the controller in the nominal plant (parameters in Hata! Başvuru kaynağı bulunamadı. , Hata! Başvuru kaynağı bulunamadı. and Hata! Başvuru kaynağı bulunamadı.) against wide range of the load variation as an external disturbance is investigated using the proposed feedback linearization controller. During simulation, the fuel cell is forced by severe changes of the load current involving 100 to 150 Amps at twentieth second. Again in the fifty fifth second the current is decreased from 150 Amps to 120 Amps. Finally, in the eightieth second the current is again increased from 120 Amps to 190 Amps (Figure 7). In order to regulate and stabilize  $\lambda_{o_2}$  at a set point, the outlet flow rate of the air compressor is measured using a (0-15 Slpm) flow meter. In this case, the measurement delay of  $W_{cp}$  is ignored where Figures 8 and 10 show the outcome. Figure 8 depicts the tracking of  $\lambda_{o_2}$  vs. different load conditions which confirms the performance of the proposed control. The tracking time is about 0.7 seconds when a change in the load occurs. The behavior of the voltage of the compressor as the control input is also depicted in Figure 9. The robustness of the proposed controller is compared in the simulation with a second order sliding mode as another robust controller. The super twisting controller produces a control law  $u$  with two terms without the need for information on  $\dot{x}$ . The first term is a discontinuous time derivative function, whilst the second term is of a continuous sliding variable as in the following:

$$u=-a |S|^{\frac{1}{2}} \text{sign}(S)-b \int_0^t \text{sign}(S(\tau)) d\tau \quad (38)$$

Where  $a$  and  $b$  are the design parameters. This controller with relative degree of one provides proper performance together with satisfactory robustness against disturbances and uncertainties [31]. Furthermore, this is found effective for chattering attenuation purpose. The super twisting controller parameters are tuned to have a low content of high frequency components in the control. After an iterative refining procedure, the following proper sets of parameters are chosen:

$$a =0.5, b =0.2 \quad (39)$$

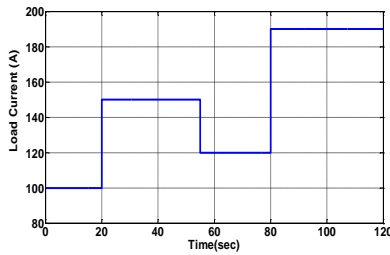


Figure 7: Profile of the load current changes

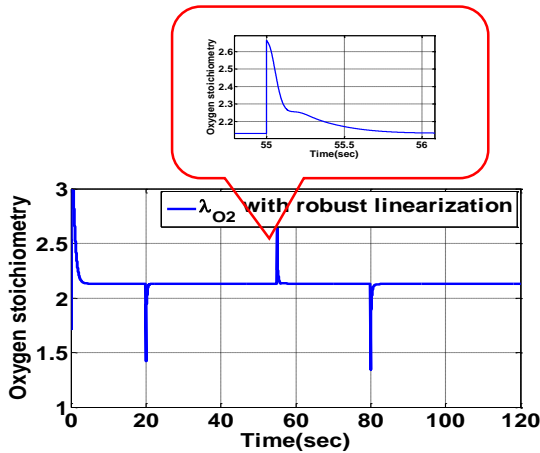


Figure 8: The controlled oxygen excess ratio  $\lambda_{O_2}$  using the robust feedback linearization ignoring the measurement delay

The controlled oxygen excess ratio in response to the load variation can be seen in **Hata! Başvuru kaynağı bulunamadı.** when the air flow is considered without delay. As shown in Figure 10, the tracking is made possible in less than 3 seconds. In contrast, Figure 10 shows the superiority of the feedback linearization when achieves the tracking in 0.7 second.

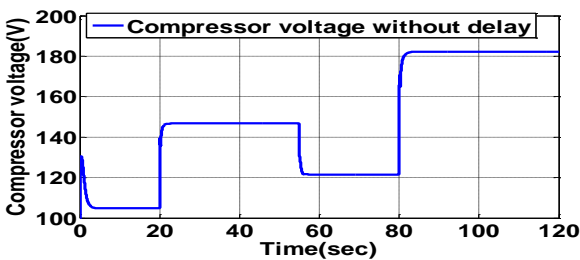


Figure 9: The control input (the voltage of the compressor) using the robust feedback linearization

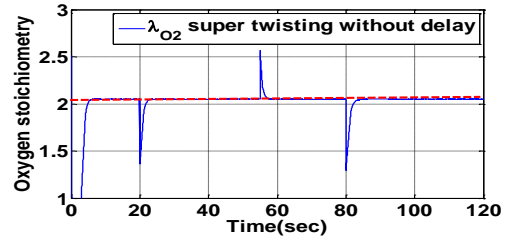


Figure 10: The controlled oxygen excess ratio  $\lambda_{O_2}$  with super twisting algorithm ignoring the measurement delay

As a practical investigation, a delay of one second is considered when  $w_{cp}$  i.e. the air flow of the compressor is measured. Both of the second order sliding mode with super twisting algorithm and robust feedback linearization controllers are gained considering the delay of one second. Outcomes are given in Figures 11 and 13 respectively. Those Figures again confirm superiority of the robust feedback linearization controller with respect to the second order sliding mode when the tracking of  $\lambda_{O_2}$  is done at a desired command. The tracking of  $\lambda_{O_2}$  using super twisting algorithm is seen oscillating. Since the air flow is directly affected by the angular velocity, the speed oscillation causes oscillation in the outlet air flow of the compressor. Likewise, the measurement delays cause oscillations using the super-twisting controller.

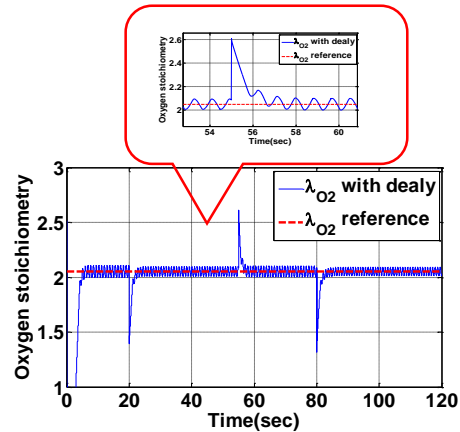


Figure 11: Control of  $\lambda_{O_2}$  with super twisting algorithm with delay

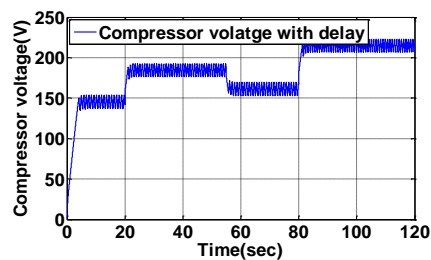


Figure 12: The compressor voltage with super twisting algorithm with delay

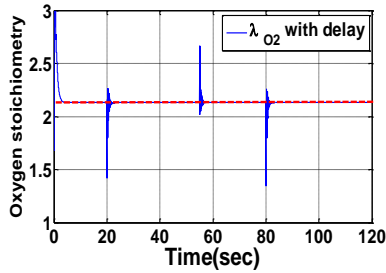


Figure 13: Control of  $\lambda_{O_2}$  using the robust feedback linearization with delay

This again excites un-modeled dynamics because of higher frequency in the oscillations. The un-modeled dynamic again increases the chattering with 1.25 rad/s frequency and 0.04 in the amplitude when a super twisting controller is used as seen in Figure 14. It can be seen that the measurement delay causes an instability of the controller. From the simulation can be seen that there is a severe impulse in  $\lambda_{O_2}$ . This phenomenon reduces the life time of the fuel cell whilst increases the consumption of the energy and the power. The differential pressure (between the anode and cathode) of both sides of the membrane must be kept small (lower than 500 mbar) to avoid damage to the membrane due to large oscillations. A 1 second delay of the sensor in the outlet air flow reduces the efficiency of the tracking and control of  $\lambda_{O_2}$ . However, the robust feedback linearization controller is seen a good choice to prevent the oscillation in the tracking. Behavior of the voltage compressor using second order sliding mode with super twisting algorithm under different load conditions is depicted in Figure 12. The figure shows high frequency oscillation in the compressor voltage. These oscillations lead to a physical damage in the membrane. This is because oscillations at the cathode side produces wider differential pressure at the cathode and anode sides and damages the membrane. Furthermore, the high frequency switching destructs the electrical motor and the compressor.

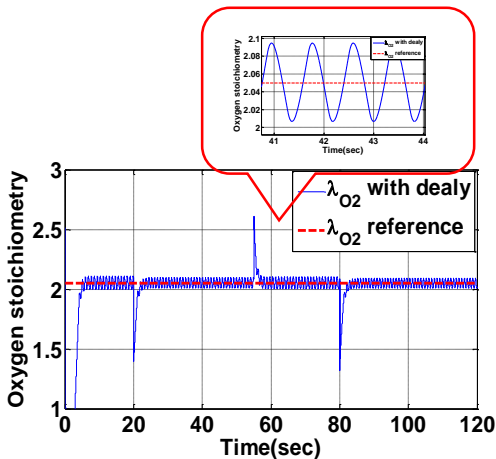


Figure 14: Control of  $\lambda_{O_2}$  with super twisting algorithm with delay and un-modeled dynamic

Figure 15 exhibits the dynamic behavior of the stack voltage vs. changing the load current. It is shown that the fuel cell voltage is a function of the current, reactant partial pressure, and membrane humidity. The voltage model contains an equation that depends on varying fuel cell variables such as current, reactant gas partial pressures and membrane humidity.

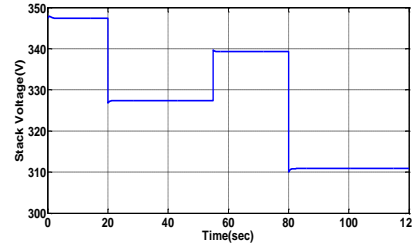


Figure 15: Stack voltage under the load current variation

### 4.2. Effect of the controller in the presence of parametric uncertainty

Performance of the proposed robust feedback linearizing controller against parametric uncertainty is investigated. Practically parameters of PEMFC are hard to spot. These parameters are dependent to environmental conditions such as temperature, structural characteristics of stacks such as manifolds volume, cathode volume, rotor inertia, and etc. A permissible bound of variation is reported in **Hata! Başvuru kaynağı bulunamadı.** Kunusch et al. [16]. An importance of the feedback linearizing controller is verified through the simulation. Apart from the impulse of due to the sudden changes in the load condition, the robust feedback linearizing scheme effectively controls the tracking of  $\lambda_{O_2}$  as shown in Figure 16. In order to spot the ability of the robust controller a stochastic uncertainty is applied on the ambient temperature. The following section deals with the time varying uncertainty control issue.

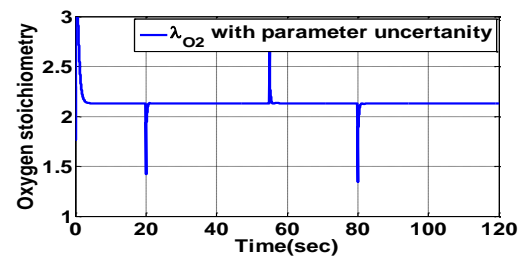


Figure 16: Control of  $\lambda_{O_2}$  using the robust feedback linearization in the presence of parametric uncertainty

### 4.3. Stochastic uncertainty in the ambient temperature

In order to signify capability of the proposed robust controller, a practical measurement noise is applied to the ambient temperature where the oxygen excess ratio  $\lambda_{O_2}$ , is

controlled in the presence of this stochastic uncertainty in the temperature, similar to [16] as in (Table7).

**- The uncertainty characteristics**

Some measurement noise are collected from a practical real application using 1710 HG Advantech™ card in association with the MATLAB™ similar to RakhtAla et al.[32] which can be seen in Figure 17. Features of collected noise are extracted as seen in Table 1.

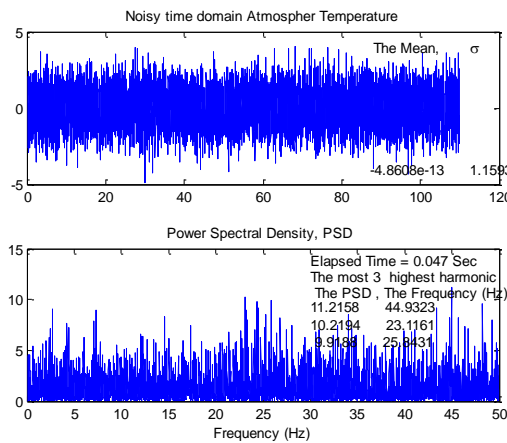


**Figure 18:** Effect of the stochastic uncertainty on the actual temperature

**- The effect of the uncertainty on the actual temperature and to the stoichiometry**

The frequency spectrum of uncertainty can be seen here in Figure 17 for the atmosphere temperature from and likewise in Figure 18 for the Stoichiometry i.e.  $\lambda_{O_2}$ . As can be seen from Figure 17, the temperature varies in bound of [-4.8669, 4.0007] in a random (uniform) way which seems huge. The temperature is a key issue to control PEMFC [4-6]. It, therefore, degrades the stoichiometry control to remain constant as it was supposed to be [4-6]. The lack of control can be observed in Figure 18 while generates an oscillatory (random) response in  $\lambda_{O_2}$ . The degradation of the stoichiometry can be seen in both of the time domain (top) and in the frequency spectrum in (below) Figure 18. However, it seems the designed robust controller performs the undertaken duty well enough when the higher frequency component of the signal (above 5 Hz) is band passed. Furthermore, the amplitude of the oscillation is attenuated from 4.0007 to 0.0089 for the maximum criteria as an index of quality. The same happens for other indices than the "max". Performance of the controller will be signified if the energy is chosen as an index. In this case the energy of the perturbation signal (in terms of the highest frequency component i.e. the 1<sup>st</sup> harmonic) is dramatically attenuated from 44.9323 at 11.2158 Hz to 0.6454 at 0.00012782 Hz (almost DC). This shows 69.6193 reduction in the energy. Specification of the perturbed and controlled  $\lambda_{O_2}$  can be observed from Figure 18 and also in table 9. However, if someone intents to finds the global

sensitivity issue of the controller, i.e.  $(S_{\lambda}^T = \frac{\partial T}{\partial \lambda} \lambda = \frac{\Delta T / T}{\Delta \lambda / \lambda})$ , it is evaluated by the "Max/Nominal" index in tables which assessed  $0.0040/0.0134 = 0.2985$ . This clarifies capability of the designed robust controller when reduces the sensitivity by a third ratio.

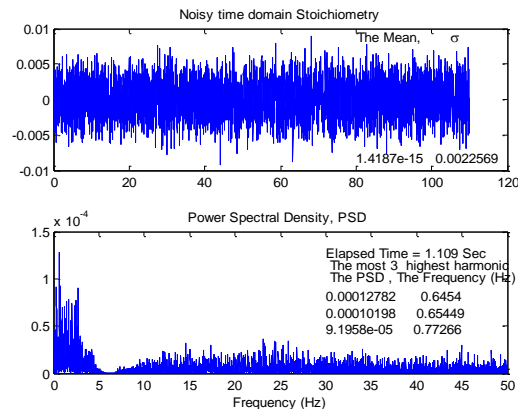


**Figure 19:** Effect of the stochastic uncertainty on the stoichiometry control

**5. Conclusions**

In the current work, a robust feedback linearization control approach based on the gap metric analysis is used to stabilize  $\lambda_{O_2}$  at a desired optimal point. The gap metric method is applied in this paper to assess the difference between the perturbed plants and the nominal plant. Model of the fuel cell is proposed as a nominal plant incorporates a dynamic of six states. Capability of the proposed controller is assessed in the presence of the large load variation. Significance of the robust feedback linearization is seen over the second order sliding mode controller when the former provides faster transient and steady state response. The latter i.e. the sliding mode controller produces an oscillatory response of the angular velocity that leads to oscillation in the outlet air flow of compressor and as a result lead to oscillation in the stoichiometry. Simulation result verifies that the stoichiometry control i.e.  $\lambda_{O_2}$  is successfully performed at the desired set point. Simulation results are shown that the measurement delay causes oscillations using the super-twisting controller. This again excites un-modeled dynamics because of higher frequency in the oscillations. The proposed controller eliminates influence of un-modeled dynamic and delay of actuator and sensor. Furthermore the performance of the proposed robust controller is confirmed under parametric uncertainty. Therefore, the proposed controller prolongs the PEMFC life time when a well-behave tracking of  $\lambda_{O_2}$  is made possible. Further investigation is performed when a practical stochastic uncertainty is applied on the ambient temperature. The proposed robust controller is shown capable of tuning  $\lambda_{O_2}$ . Furthermore, the controller reduces the global sensitivity against the measurement noise by a third factor.

## 6. References

- [1] Larminie, J., Dicks, A., "Fuel Cell Systems Explained", 2nd ed. New York: SAE International and John Wiley & Sons, 2003.
- [2] Li, Q., Chen, W., Wang, Y., Jia, J., Han, M., "Nonlinear robust control of proton exchange membrane fuel cell by state feedback exact linearization", *Journal of Power Sources*, vol. 194, pp. 338-348, 2009.
- [3] Matraji, I., Laghrouche, S., Jemei, S., Wack, M., "Robust control of the PEM fuel cell air-feed system via sub-optimal second order sliding mode", *Applied Energy*, vol. 104, pp. 945-957, 2013.
- [4] Grujicic, M., Chittajallu, K. M., Pukrushpan, J., "Control of the transient behaviour of polymer electrolyte membrane fuel cell systems", *Proceedings of the Institution of Mechanical Engineers, Part D: Journal of Automobile Engineering*, vol. 218, pp. 1239-1250, 2004.
- [5] Peng, H., Pukrushpan, J., "Control of Fuel Cell Power Systems: Principle, Modeling, Analysis and Feedback Design", Berlin, Germany Springer-Verlag, 2004.
- [6] Pukrushpan, J., Stefanopoulou, A., Peng, H., "Control of Fuel Cell Breathing", *Control Systems Magazine*, pp. 30-46, 2004.
- [7] Grujicic, M., Chittajallu, K., Law, E., Pukrushpan, J., "Model-based control strategies in the dynamic interaction of air supply and fuel cell", *Proceedings of the Institution of Mechanical Engineers, Part A: Journal of Power and Energy*, vol. 218, pp. 487-499, 2004.
- [8] Na, W. K., Gou, B., Diong, B., "Nonlinear Control of PEM Fuel Cells by Exact Linearization", *IEEE Transactions on Industry Application*, vol. 43, pp. 1426-1433, 2007.
- [9] W. K. Na and B.Gou, "Feedback-Linearization-Based Nonlinear Control for PEM Fuel Cells", *IEEE Transactions on Energy Conversion*, vol. 23, pp. 179-190, 2008.
- [10] Rodatz, S., Paganelli, G., Guzzella, L., "Optimizing air supply control of a PEM fuel cell system", *In American Control Conference*, vol.3, pp. 2043-2048, 2003.
- [11] Niknezhadi, A., Allué-Fantova, M., Kunusch, C., Ocampo-Martínez, C., "Design and implementation of LQR/LQG strategies for oxygen stoichiometry control in PEM fuel cells based systems", *Journal of Power Sources*, vol. 196, pp. 4277-4282, 2011.
- [12] Garcia-Gabin, W., Dorado, F., Bordons, C., "Real-time implementation of a sliding mode controller for air supply on a PEM fuel cell", *Journal of Process Control*, vol. 20, pp. 325-336, 2010.
- [13] Talj, R.J., Hissel, D., Ortega, R., Becherif, M., Hilaiet, M., "Reduced-Order Model and a Higher-Order Sliding-Mode Control of the Air Supply System of a Proton-Exchange-Membrane Fuel Cell with Experimental Validation", presented at the 8th IEEE International Conference of Advanced Electromechanical Motion Systems & Electric Drives, Lille, 2009.
- [14] Talj, R., Hilaiet, M., Ortega, R., "Second order sliding mode control of the moto-compressor of a PEM fuel cell air feeding system, with experimental validation", *In 35th Annual Conference of IEEE Industrial Electronics, IECON '09.*, pp. 2790-2795, 2009.
- [15] Talj, R.J., Hissel, D., Ortega, R., Becherif, M., Hilaiet, M., "Experimental Validation of a PEM Fuel Cell Reduced Order Model and a Moto-Compressor Higher Order Sliding Mode Control", *IEEE Transactions on Industrial Electronics*, vol. 57, pp. 1906-1913, 2010.
- [16] Kunusch, C., Puleston, P.F., Mayosky, M.A., Riera, J., "Sliding Mode Strategy for PEM Fuel Cells Stacks Breathing Control Using a Super-Twisting Algorithm", *IEEE Transactions on Control Systems Technology*, vol. 17, pp. 167-174, January 2009.
- [17] Kunusch, C., Puleston, P.F., Mayosky, M.A., Serra, M., "Advances in HOSM control design and implementation for PEM fuel cell systems", *In 14th International Conference on Methods and Models in Automation and Robotics, Miedzyzdroje, Poland*, pp. 709-716, 2009.
- [18] Kunusch, C., Puleston, P., Mayosky, M., Davila, A., "Efficiency Optimization of an Experimental PEM Fuel Cell System via Super Twisting Control", *In 11th IEEE Conference of Variable Structure Systems, Mexico City, Mexico*, pp. 319-324, 2010.
- [19] Rakhtala Rostami, S. M., Noei, A. R., Gaderi, R., "Control of PEM fuel cell system via higher order sliding mode control", *International Journal of Automation and Control*, vol. 6, pp. 310-329, 2012.
- [20] Kunusch, C., Puleston, P. F., Mayosky, M. A., Fridman, L., "Experimental results applying second order sliding mode control to a PEM fuel cell based system", *Control Engineering Practice*, vol. 21, pp. 719-726, 2013.
- [21] Pukrushpan, J., Peng, H., Stefanopoulou, A., "Simulation and analysis of transient fuel cell system Performance based on a dynamic reactant flow model," *In ASME International Mechanical Engineering Conference and Exposition, USA*, pp. 1-12, 2002.
- [22] Rakhtala, S.M., Ghaderi, R., Ranjbar Noei, A., "Proton exchange membrane fuel cell voltage-tracking using artificial neural networks", *Journal of Zhejiang University Science C*, vol. 12, pp. 338-344, 2011.
- [23] Pisano, A., Salimbeni, D., Usai, E., Rakhtala, S. M., Noei, A. R., "Observer-based output feedback control of a PEM fuel cell system by high-order sliding mode technique", *In European Control Conference (ECC) 2013*, pp. 2495-2500, 2013.
- [24] Kunusch, C., Puleston, P.F., Mayosky, M.A., Husar, A.P., "Control-Oriented Modeling and Experimental Validation of a PEMFC Generation System", *IEEE Transaction on Energy Conversion*, vol. 28, pp. 851-861, 2011.
- [25] Isidori, A., "Nonlinear Control Systems", London, England: Springer-Verlag, 1996.
- [26] Franco, A. L. D., Bourles, H., De Pieri, E. R., Guillard, H., "Robust nonlinear control associating robust feedback linearization and  $H_\infty$  control", *IEEE Transactions on Automatic Control*, vol. 51, pp. 1200-1207, 2006.
- [27] Wang, F., Chen, H., Yang, Y., Yen, J., "Multivariable robust control of a proton exchange membrane fuel cell system", *Journal of Power Sources*, vol. 177, pp. 393-403, 2008.
- [28] Wang, F., Ko, C., "Multivariable robust PID control for a PEMFC system", *International journal of hydrogen energy*, vol. 35, pp. 437-445, 2010.
- [29] Wang, F., Chen, H., "Design and implementation of fixed-order robust controllers for a proton exchange membrane fuel cell system", *International journal of hydrogen energy*, vol. 34, pp. 2705-2717, 2009.
- [30] McFarlane, D. C., Glover, Keith, "Robust controller design using normalized co-prime factor plant descriptions", *Lecture Notes in Control and Information Sciences*, Springer Verlag, New York, USA, vol. 138, 1990.
- [31] Pisano, A., Usai, E., "Sliding mode control: A survey with applications in math", *Mathematics and Computers in Simulation*, vol. 81, pp. 954-979, 2011.
- [32] Rakhtala, S.M., Ghaderi, R., Ranjbar, A., Usai, E., "Design of Finite-time High-Order Sliding Mode State Observer; a Practical Insight to PEM Fuel Cell System", *Journal of Process Control*, vol. 24(1), pp.203-224, 2014.

**Table 5:** Linearized transfer functions of the PEMFC at different operating points

$G_1 = \frac{(s + 89.08)(s + 39.68)(s + 3.075)(s^2 + 1.891s + 0.964)}{(s + 89.07)(s + 39.64)(s + 3.909)(s + 3.067)(s^2 + 2.369s + 1.494)}$ $I_{st} = 100; u = 150; x_{10} = 8650; x_{20} = 1.634 \times 10^5; x_{30} = 0.03215; x_{40} = 1.627 \times 10^{-3}; x_{50} = 8.91 \times 10^{-3}; x_{60} = 1.35 \times 10^5$
$G_2 = \frac{(s + 88.84)(s + 39.47)(s + 2.949)(s + 1.046)(s + 0.9157)}{(s + 88.84)(s + 39.43)(s + 3.846)(s + 2.93)(s^2 + 2.487s + 1.547)}$ $I_{st} = 200; u = 150; x_{10} = 8738; x_{20} = 1.577 \times 10^5; x_{30} = 0.0314; x_{40} = 6.05 \times 10^{-4}; x_{50} = 9.245 \times 10^{-3}; x_{60} = 1.313 \times 10^5$
$G_3 = \frac{(s + 88.68)(s + 39.38)(s + 2.865)(s^2 + 1.99s + 1.002)}{(s + 88.68)(s + 39.35)(s + 3.808)(s + 2.847)(s^2 + 2.533s + 1.627)}$ $I_{st} = 250; u = 150; x_{10} = 8780; x_{20} = 1.55 \times 10^5; x_{30} = 0.0311; x_{40} = 8.02 \times 10^{-5}; x_{50} = 9.436 \times 10^{-3}; x_{60} = 1.291 \times 10^5$
$G_4 = \frac{(s + 88.94)(s + 39.52)(s + 3.029)(s^2 + 1.532s + 0.6518)}{(s + 88.93)(s + 39.49)(s + 3.92)(s + 3.026)(s^2 + 2.004s + 1.016)}$ $I_{st} = 50; u = 150; x_{10} = 8615; x_{20} = 1.637 \times 10^5; x_{30} = 0.0325; x_{40} = 2.125 \times 10^{-3}; x_{50} = 8.763 \times 10^{-3}; x_{60} = 1.383 \times 10^5$

**Table 6:** The gap metric of all transfer functions

	G <sub>1</sub>	G <sub>2</sub>	G <sub>3</sub>	G <sub>4</sub>
G <sub>1</sub>	0	0.0031	0.0024	0.0019
G <sub>2</sub>	0.0031	0	9.75 × 10 <sup>-4</sup>	0.0018
G <sub>3</sub>	0.0024	9.75 × 10 <sup>-4</sup>	0	0.0018
G <sub>4</sub>	0.0019	0.0018	0.0018	0
Max	0.0031	0.0031	0.0024	0.0019
Min				0.0019

**Table 7:** Bound of parameter variations Kunusch et al. [16]

Parameter	Variation
1. Stack Temperature (T <sub>st</sub> )	1. ±10 %
2. Cathode Volume (V <sub>cm</sub> )	2. ±5 %
3. Supply manifold volume (V <sub>sm</sub> )	3. ±10 %
4. Return manifold volume (V <sub>rm</sub> )	4. ±10 %
5. Ambient Temperature (T <sub>amb</sub> )	5. ±10 %
6. Motor Inertia (J <sub>cp</sub> )	6. ±10 %
7. Compressor Diameter(dc)	7. ±1 %

**Table 8:** Characteristics of applied noisy uncertainty

Nominal Temperature	Min. Variation	Max. Variation	std	Max/Nominal	Distribution
298 <sup>o</sup> K	-4.8669	4.0007	1.1593	1.34%	Uniform

**Table 9:** Specification of the controlled the Stoichiometry

Nominal Set point	Min. Variation	Max. Variation	std	Max/Nominal	Distribution
2.25	-0.0091	0.0089	0.0022569	0.4%	Gaussian

## Appendix I: Model Parameters in Tables 2-4

Table 2: General parameters in the modeling of PEMFC

Parameter	symbol	SI Units	Value
Atmospheric pressure	$P_{atm}$	Pa	101325
Average ambient air relative humidity	$\Phi_{atm}$	--	0.5
Saturation pressure	$P_{sat, Tatm}$	Pa	$3.1404 \times 10^3$
Atmospheric temperature	$T_{atm}$	K	298.15
Air-specific heat ratio	$\gamma$	--	1.4
Air density	$C_p$	J/kg/K	1004
Universal gas constant	$R$	J/mol/K	8.31451
Air gas constant	$R_a$	J/mol/K	286.9
Oxygen gas constant	$R_{O2}$	J/kg/K	259.8
Nitrogen gas constant	$R_{N2}$	J/kg/K	296.8
Vapor gas constant	$R_v$	J/kg/K	461.5
Molar mass of air	$M_a$	kg/mol	$28.97 \times 10^{-3}$
Molar mass of oxygen	$M_{O2}$	kg/mol	$32 \times 10^{-3}$
Molar mass of nitrogen	$M_{N2}$	kg/mol	$28 \times 10^{-3}$
Molar mass of vapor	$M_v$	kg/mol	$18.02 \times 10^{-3}$
Faraday's constant	$F$	C/mol	96487
Temperature of the fuel cell	$T_{fc}$	K	353
Maximum mass of vapor in cathode	$m_{v, ca, max}$	kg	0.002889
Humidity ratio	$\Omega_{atm}$	--	--
Temperature of the return manifold	$T_{rm}$	K	--

Table 3: Parameters in the modeling of PEMFC

Parameter	symbol	SI Units	Value
Motor constant	$K_t$	Nm/A	0.0153
Motor constant	$R_{cm}$	ohm	0.82
Motor constant	$K_v$	V/(rad/sec)	0.0153
Compressor efficiency	$\eta_{cp}$	--	0.8
Compressor motor mechanical efficiency	$\eta_{cm}$	--	0.98
Compressor diameter	$dc$	m	0.2286
Compressor and motor inertia	$J_{cp}$	N.m	$2 \times 10^{-7}$
Number of cells in fuel cell stack	$n$	--	381
Fuel cell active area	$A_{fc}$	m <sup>2</sup>	$280 \times 10^{-4}$
Supply manifold volume	$V_{sm}$	m <sup>3</sup>	0.02

Single stack cathode volume	$V_{ca}$	$m^3$	0.005
Return manifold volume	$V_{rm}$	$m^3$	0.005
Supply manifold outlet orifice constant	$K_{sm,out}$	$kg/sec/Pa$	$0.3629 \times 10^{-5}$
Cathode outlet orifice constant	$K_{ca,out}$	$kg/sec/Pa$	$0.2177 \times 10^{-5}$
Oxygen mole fraction at cathode inlet	$y_{O2,in}$	--	$\frac{X_{O2,in} M_{O2}}{M_a^{atm}}$
Oxygen mole fraction in dry air	$X_{O2,in}$	--	0.21

**Table 4:** Polynomial coefficients of equations

$\beta_{00}$	$4.83 \times 10^{-5} \text{ kg/sec}$	$P_{a6}$	0.07804	$\alpha_{00}$	0
$\beta_{10}$	$-5.42 \times 10^{-5} \text{ kg/sec}^2$	$P_{a5}$	0.02772	$\alpha_{10}$	0.0058 $N m \text{ sec}$
$\beta_{20}$	$8.79 \times 10^{-6} \text{ kg/sec}^3$	$P_{a4}$	0.002122	$\alpha_{20}$	- 0.0013 $N m \text{ sec}^2$
$\beta_{01}$	$3.49 \times 10^{-7} \text{ kg/sec}^2/\text{bar}$	$P_{a3}$	- 0.001524	$\alpha_{01}$	$3.25 \times 10^{-6} \text{ N m / bar}$
$\beta_{11}$	$3.55 \times 10^{-13} \text{ kg/sec}$	$P_{a2}$	- 0.001967	$\alpha_{11}$	- $2.80 \times 10^{-6} \text{ N m sec / bar}$
$\beta_{02}$	$-4.11 \times 10^{-10} \text{ kg/sec / bar}$	$P_{a1}$	0.001248	$\alpha_{02}$	- $1.37 \times 10^{-9} \text{ N m sec / bar}^2$
$c_1 = \frac{R_{N2} T_{st}}{V_{ca}}$		$c_2 = \frac{R_{O2} T_{st}}{V_{ca}}$		$\alpha_1$	$3.92 \times 10^{-6} \text{ N m sec}$
$c_3 = \frac{P_{v,ca} V_{ca} M_v}{R_v T_{st}}$				$\alpha_0$	$4.1 \times 10^{-4} \text{ N m}$

**Note:**



**Dr. Seyed Mehdi Rakhtala,**

He was born in Iran in 1976. He received his B.S. degree in electrical engineering in Iran. The M.S. degree from Mazandaran University in Iran in 2006. He has taken the Ph.D. degree of control engineering from the Electrical Engineering Department, Mazandran university in 2012. During 2004-2008, he was head of electrical and electronic in the fuel cell Research center. At now, He is Head of Electrical and Electronic Department and Assistant Prof. of Golestan University.